7

Adaptive Ground Penetrating Radar Systems to Visualize Antipersonnel Plastic Landmines Based on Local Texture in Scattering / Reflection Data in Space and Frequency Domains

Yukimasa Nakano and Akira Hirose
Department of Electrical Engineering and Information Systems, The University of Tokyo
Japan

1. Introduction

Ground penetrating radars (GPRs) are widely used for buried object search, ruin investigation, groundwater assessment, and other various applications (Sato & Takeshita, 2000) (Moriyama et al., 1997). They are also expected to find nonmetallic landmines (Bourgeois & Smith, 1998) (Montoya & Smith, 1999) (Peters Jr. & Daniels, 1994) (Sato et al., 2004) (Sato, 2005) (Sato et al., 2006). Figure 1 shows the size and the structure of a plastic antipersonnel landmine. A near future target is to find or visualize antipersonnel landmines with a high distinction rate between landmines and other objects. The conventional metal detectors, based on electromagnetic induction, use so low frequency that the electromagnetic field penetrates through the soil very deep, and the false negative probability is very small. However, because of its long wavelength, the resolution is limited, and they can tell just whether inductive material exists or not. They cannot distinguish landmines from other metal fragments. GPRs employ much higher frequency. Then the resulting higher resolution will be helpful to discriminate landmines.

Currently, there are two methods to remove the plastic landmines. One is a metal detector, and the other is a rotary cutter. The former detects a blasting cap made of metal in the landmine. Because the cap is very small, we must set the sensitivity at a high level. Then, the positive fault rate is as high as about 99.9% (specificity=0.1%), resulting in a lot of time to remove the landmines. The latter, rotary cutter, looks like a bulldozer, bores the ground and tries to clear the landmines by exploding them. The problems in this method are necessity of additional removal by human because of impossibility of perfect clearance, necessity of sufficient areas for the approach of the rotary cutter, and land pollution by the exploded powder.

Accordingly, though these methods have certain merits, they have also demerits. Therefore, new landmine detection systems based on GPRs attract attention and are studied by a dozen of researcher groups/laboratories presently to solve the problem. Most of the proposed methods employ high-frequency and wide-band electromagnetic wave to visualize a plastic landmine itself instead of the metallic blasting cap. There are two types among the

Fig. 1. The size and the structure of a plastic antipersonnel landmines.

proposals. Some employ pulsed electromagnetic wave and others employ stepped-frequency continuous wave. We explain these two measurement methods in detail in the next section.

Unlike the metal detector which measures induced current, GPRs observe the reflected and scattered electromagnetic wave. In general, it is noted that the electromagnetic wave is reflected at boundaries between materials having different permittivity, and that the spatial resolution of the observation is almost the same as the wavelength. Therefore, it is possible to detect not only the metal but also the plastic body because the electromagnetic wave is reflected at the boundary of the soil and the plastic. In addition, the wide band electromagnetic wave has the possibility to observe the the accurate distance from the antenna to the target, physical property for electromagnetic wave and structural characteristics of the target. That is to say, a GPR system has a potential of detecting plastic landmines more strictly than the metal detector does.

However, high-frequency wave also induce a lot of clutter, which is caused by the roughness of the earth's surface and scattering substances other than the plastic landmines. Consequently, it is very difficult to extract significant features helpful for detecting the plastic landmines from the observed data by ignoring the clutter. Furthermore, it is also difficult to treat the extracted features effectively. A lot of processing methods were proposed so far. That is, we must resolve the following two steps to detect the plastic landmines. The first step is how to extract the features, and the second is how to treat the extracted features. To accomplish our goals, we must select or develop new effective methods.

Previously we proposed an adaptive radar imaging system to visualize plastic landmines using complex-valued self-organizing map (CSOM) (Hara & Hirose, 2004) (Hara & Hirose,

2005). With the system, we observe reflection and scattering to obtain a complexamplitude two-dimensional image at multiple frequencies. In the resulting 3-dimensional (2-dimensional (space) × frequency) data, we extract local texture information as a set of feature vectors, and feed them to a CSOM for adaptive classification of the 3-dimensional texture (Hirose, 2006) (Hirose, 2003). By using the system, we could visualize antipersonnel plastic landmines buried shallowly underground. We also constructed a preliminary object identifier, which is a type of associative memory that learns the feature of the plastic-landmine class with adaptation ability to various ground conditions (Hirose et al., 2005).
However, the system requires a long observation time because it employs mechanical scan. Long observation time is one of the most serious problems in high-resolution imaging systems. Some methods to overcome the problem have been investigated (Kobayashi et al., 2004) (Shrestha et al., 2004).
We then developed a portable visualization system with an antenna array to reduce the observation time (Masuyama & Hirose, 2007). The array has 12×12 antenna elements, resulting in about 144 pixels. The element aperture size is 28mm×14mm, which determines the spatial resolution. In texture evaluation and adaptive CSOM classification, a higher resolution leads to a better performance. We recently proposed a resolution enhancement method using a special antenna-selection manner in combination with elimination of direct coupling and calibration of propagation pathlength difference (Masuyama et al., 2007).
However, even with such resolution enhancement, the visualization performance is still worse than that obtained with the first mechanical-scanning system. The resolution is still insufficient, and the mutual coupling between antenna elements are not completely ignorable.
In this chapter, we propose two techniques to improve the visualization ability without mechanical scan, namely, the utilization of SOM-space topology in the CSOM adaptive classification and a feature extraction method based on local correlation in the frequency domain. In experimental results, we find that these two techniques improve the visualization performance significantly. The local-correlation method contributes also to the reduction of tuning parameters in the CSOM classification.
The organization of this chapter is as follows. In Section 2, we explain the merits and demerits of three plastic landmine detection systems that utilize the electromagnetic technology. Then we show the processing flow of our plastic landmine detection system based on the CSOM and show the conventional and proposal methods in Section 3. In Section 4, we show the experimental results with the observed data. Finally, we summarize and conclude this chapter in Section 5.

2. Conventional technology

As mentioned before, there are three methods which utilize the electromagnetic technology to detect plastic landmines. One is the metal detector based on induction current, another is the pulse radar using the electromagnetic wave, the other is stepped-frequency radar using the electromagnetic wave. In the following subsections, we briefly explain the characteristics of these methods respectively.

2.1 Metal detector

The fundamental principle of the metal detector is to sense the mutual interaction between a coil of the detector and target conductors using low frequency electromagnetic field induced

by the coil. The used frequency is from about f = 100kHz to 1MHz. Because the frequency is very low, the metal detector is highly tolerant against inhomogeneous ground and the depth of the buried landmines. Additionally, it is very easy to manufacture a highly sensitive metal detector because it consists of some simple analog oscillation circuits. Consequently, the metal detector is very suitable for landmine detection, where we expect not to miss landmine at all, and this method is widely used for the current landmine detection.
However, it is impossible for the metal detector to detect targets other than conductors and difficult to search a target with a high spatial resolution because of the long wavelength. In addition, we cannot obtain the time and/or frequency response which shows the features originating at the targets because the bandwidth is very narrow. The most critical problem is the very high probability of the positive fault which is caused by the metal scattering substance. In particular, as the landmines are buried in a field of combat, there are a large amount of metal fragments around buried landmines, and according to a report, the positive fault is about 99.9%. Therefore, it takes long time to remove landmines perfectly, which is a very big problem. In addition, when we use multiple metal detectors simultaneously, improper signals are often caused by the mutual coupling among closely located detectors.

2.2 Pulse GPR

A pulse GPR observes the time response of the electromagnetic-wave pulse irradiated toward the ground. The time response represents the depth of a scatterer. When we sweep an antenna in two dimension horizontally, we can obtain the three dimensional data. Besides, as the electromagnetic wave is reflected at the boundary of materials that have different permittivity, it is possible to observe the reflection wave from the plastics that forms a landmine, not only the metal blasting cap. The pulse GPRs have another merit. As the pulse have a wide bandwidth, as wide as that of the stepped-frequency range mentioned below, we can observe not only the time response but also the frequency response through the Fourier transform, and these data may show characteristics of the target. Regarding the measuring time, we can conduct the measurement more speedily in comparison with the stepped-frequency GPRs.
However, as a maximum frequency component of the pulse radar is usually about f = 6GHz at the most. That is, the shortest free-space wavelength is about 5cm. Then the pulse GPRs cannot observe sufficient amount of characteristics of plastic landmines whose size is typically the same as the wavelength. Besides, the ground surface is very rough, and the soil, including various scatterers, often causes serious clutter. Therefore, it is very difficult to obtain clear images. To solve this problem we need to utilize sharper pulse which consists of a wideband wave with a high power. However, as a high-peak pulse is distorted by the nonlinearity in transmitter circuits and switched antennas, the problem cannot be solved sufficiently.

2.3 Stepped-frequency GPR

Stepped-frequency GPRs observe the reflected continuous wave at a wide-range frequency points. This method does not need to output strong power instantaneously. Then, the electromagnetic wave has little influence on the nonlinearity of the circuits and the switches. As the results, stepped-frequency GPR accomplishes higher SN ratio than the pulse GPR. In addition, it is easier for the stepped-frequency radar to observe the high frequency wave and select bandwidth freely than a pulse radar system. Besides, we can obtain the time

response, like what pulse radar provide, through the inverse Fourier transform of the observed frequency domain data.
As above, stepped-frequency GPRs enable to accomplish high SN ratio at the high frequency with a wide band, and obtain not only the time response but also frequency domain feature very effectively. It is true that even the stepped-frequency GPR has a drawback. Namely, it takes too long time to measure the scattering because of the time required for frequency sweeping. However, this problem will be solved by inventing new appropriate devices in the near future.
Then we can expect a higher precision with the system utilizing the stepped-frequency GPR than the conventional systems. To achieve this purpose, there are two important points we should consider carefully. One is to extract useful features from the obtained data, and the other is to fully utilize the features. However, a perfect technique has not been suggested yet.
In the next section, we show the details of our CSOM-based signal processing published in our previous paper (Nakano & Hirose, 2009).

3. System construction

3.1 Overall construction

Figure 2 shows the processing flow in our plastic landmine visualization system. We describe the components briefly.

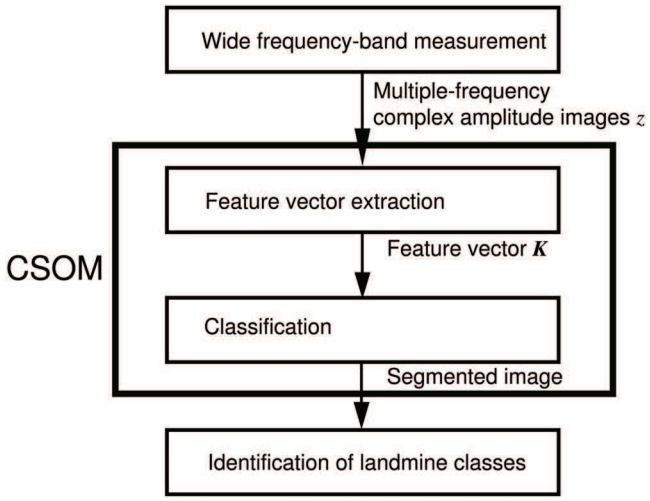

Fig. 2. The overall processing flow (Nakano & Hirose, 2009).

First, we operate our system at a stepped-frequency mode to obtain wideband electromagnetic reflection and/or scattering images at multiple frequency points. The details of the system is given in Ref.(Masuyama & Hirose, 2007). We acquire complex amplitude images at 10 observation frequency points from 8 to 11.6GHz at an interval of 0.4GHz.
Next, we generate a spatially segmented image by using a CSOM that classifies local texture adaptively. The classification consists of two steps. In the first step, we extract feature

vectors representing local complex-amplitude textural quantity in a local window that sweeps all over the image. As shown in Fig.3, we prepare a sweeping window in each frequency image at a synchronizing real-space location. We calculate correlations between pixel values in the window in terms of real-space relative distance and frequency-domain distance. We assume that the correlation values represent the texture at around the pixel at the window center, and we put the values at the center pixel as the textural feature. In the second step, we classify the extracted feature vectors adaptively by using a CSOM (Hara & Hirose, 2004). Then we color pixels correspondingly with the resulting classes to generate a segmented spatial image.

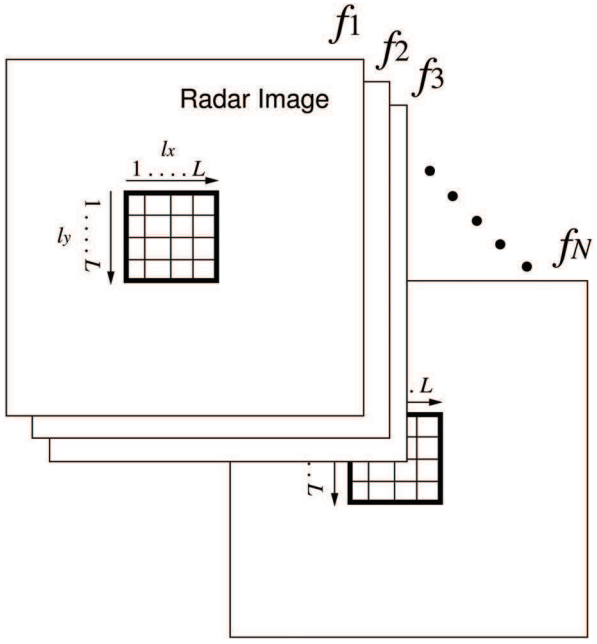

Fig. 3. The scanning window for local textural feature extraction (Nakano & Hirose, 2009).

Lastly, we identify landmine classes included in the segmented image. We use an associative memory that learns respective features of landmine classes and other objects such as metal fragments, stones and clods. We prepare a set of teacher features for the learning beforehand by observing land pieces where we know the landmine locations.

In this paper, we propose two novel methods in the CSOM processing. One is a dynamics in the feature vector classification, and the other is a feature vector extraction method. The former is utilization of SOM-space topology in the CSOM adaptive classification by introducing a ring CSOM, and the latter is the extraction of local correlation in the frequency domain.

3.2 Utilization of SOM-space topology in the CSOM adaptive classification

As the first proposal, instead of the conventional K-mean algorithm, we employ a SOM dynamics that utilizes SOM-space topology in the CSOM adaptive classification. Figure 4 shows the CSOM structure, which forms a ring in the CSOM space.

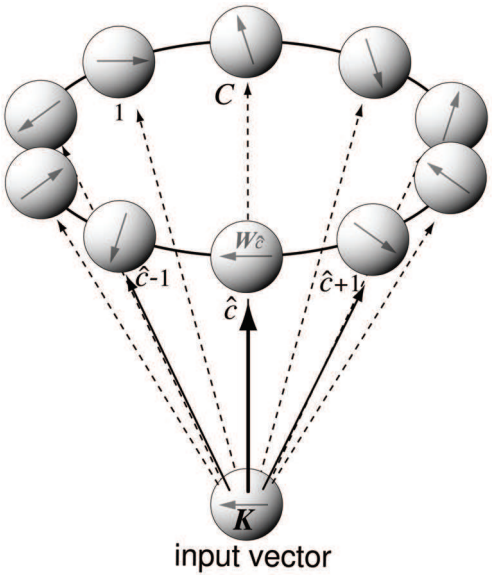

Fig. 4. The ring-CSOM structure. Balls represent reference vectors in the CSOM, and the directions of the arrows show the vector values, among which the winner $\boldsymbol{W}_{\hat{c}}$ and the two neighbors $\boldsymbol{W}_{\hat{c}\pm1}$ change in the self-organization.

In the CSOM in our previous system, we classified the feature vectors by using the K-mean clustering algorithm, which is the simplest SOM dynamics, as (Hara & Hirose, 2004)

$$\boldsymbol{W}_{\hat{c}}(t+1) = \boldsymbol{W}_{\hat{c}}(t) + \alpha(t)(\boldsymbol{K} - \boldsymbol{W}_{\hat{c}}(t)) \quad (1)$$

$$\alpha(t) = \alpha(0)\left(1 - \frac{t}{TMAX}\right) \quad (2)$$

$\boldsymbol{W}_{\hat{c}}(t)$: reference vector of the winner
$\boldsymbol{K}$: input feature vector
t : iteration number in self-organization
$TMAX$: maximum iteration number
$\alpha(t)$: self-organization coefficient
where the winner $\boldsymbol{W}_{\hat{c}}(t)$ is the reference vector nearest to $\boldsymbol{K}$ among all the reference vectors $\boldsymbol{W}_1, \boldsymbol{W}_2, \ldots, \boldsymbol{W}_c, \ldots, \boldsymbol{W}_C$. We update $\boldsymbol{W}_{\hat{c}}$ iteratively by presenting $\boldsymbol{K}$ sequentially. In the new system, we also introduce the self-organization of reference vectors at the winner neighbors ($c \pm 1$) in the SOM space shown in Fig.4 as

$$\boldsymbol{W}_{\hat{c}\pm1}(t+1) = \boldsymbol{W}_{\hat{c}\pm1}(t) + \beta(t)(\boldsymbol{K} - \boldsymbol{W}_{\hat{c}\pm1}(t)) \quad (3)$$

$$\beta(t) = \beta(0)\left(1 - \frac{t}{TMAX}\right) \quad (4)$$

where $\beta(t)$ is another self-organization coefficient for the neighboring classes, which is usually smaller than $\alpha(t)$. The classes $\hat{c} \pm 1$ are neighbors of the winner class $\hat{c}$ in the CSOM

space. The CSOM space is used only to determine the winner neighbors, whereas the winner is determined in the $\boldsymbol{K}$ space.

The reason of the modification is as follows. In the previous method, we used the K-means algorithm (1), which is the simplest dynamics in the SOM. Because we have only about 10 classes in the adaptive vector quantization in the landmine visualization system, we paid less attention to the SOM-space topology. Nevertheless, we could obtain sufficiently meaningful classification results (Hara & Hirose, 2004).

However, with the present portable visualization system with a lower spatial resolution at the antenna array (Masuyama & Hirose, 2007), the failure probability in the classification became slightly higher than the first laboratory system. We sometimes fail to extract texture features sufficiently because of the decrease in resolution. As described later, in such an insufficient extraction case, we found that only a small number of classes were used in the vector quantization.

We therefore propose the utilization of the SOM-space topology in the CSOM adaptive classification, to activate most of the prepared reference vectors, by introducing additional self-organization at neighbor class vectors. In this paper, we change the values of only the two adjacent-class vectors $\boldsymbol{W}_{c \pm 1}$ as shown in (3). The neighbor vector number is small because the number of the totally prepared classes is small, i.e., only about 10. The structure of the CSOM should also be suitable for the small size, namely, one-dimensional as shown in Fig.4.

3.3 Frequency-domain local correlation method

The second proposal is to adopt frequency-domain local correlation in the texture feature extraction. We modify the point on which we put stress based on a new concept in extracting features in the frequency domain.

Figure 5(a) illustrates the conventional method, in which the feature vector $\boldsymbol{K}$ is calculated for complex pixel values $z(l_x, l_y, f)$ as

$$\boldsymbol{K} = [M, \boldsymbol{K}_s, \boldsymbol{K}_f] \tag{5}$$

$$M = \frac{1}{L^2} \sum_{l_x=1}^{L} \sum_{l_y=1}^{L} z(l_x, l_y, f_b) \tag{6}$$

$$\boldsymbol{K}_s = [K_s(0,0), K_s(1,0), K_s(0,1), K_s(1,1)] \tag{7}$$

$$K_s(i,j) = \frac{1}{L^2} \sum_{l_x=1}^{L} \sum_{l_y=1}^{L} z(l_x, l_y, f_b) z^*(l_x + i, l_y + j, f_b) \tag{8}$$

$$\boldsymbol{K}_f = [K_f(f_1), \cdots, K_f(f_N)] \tag{9}$$

$$K_f(f_n) = \frac{1}{L^2} \sum_{l_x=1}^{L} \sum_{l_y=1}^{L} z(l_x, l_y, f_b) z^*(l_x, l_y, f_n) \tag{10}$$

where M, $\boldsymbol{K}_s$, and $\boldsymbol{K}_f$ are the mean, real-space-domain correlations, and frequency-domain correlations, respectively. Real-space discrete coordinate l_x and l_y determine pixel positions in the local window as shown in Fig.3.

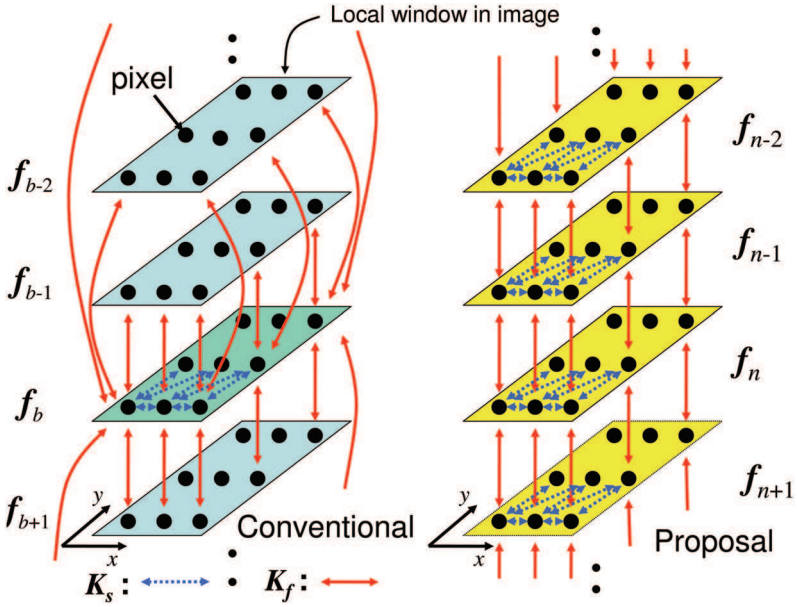

Fig. 5. (a)Conventional and (b)proposed textural feature extraction methods based on correlation in real-space and frequency domains (Nakano & Hirose, 2009).

We prepare a local observation window of $L \times L$ pixels to extract the local textural feature in the window by calculating correlations between pixel values. In (6)–(10), M is the average of pixel values in the window at a base frequency f_b, which we select among the 10- frequency observation points in advance. The vector $\boldsymbol{K}_s$ in (7) is the local correlations in the $L \times L$ real-space window at f_b, while $\boldsymbol{K}_f$ is the correlations between pixel values at f_b and other frequencies f_n at identical positions.

The effectiveness of K_f (f_n) in (10) as a feature vector was suggested by the following frequency-dependent interference. A plastic landmine usually has parallelism among its ceiling, bottom, and air gap inside, if any, which causes interference, whose spectral profile is periodic in the frequency domain. That is to say, we will observe a resonance at integral multiple of a certain frequency periodically in the frequency domain, resulting in a specific peak at certain f_n in K_f (f_n). We intended to capture this phenomenon in (10). However, we found in our series of experiments that we normally observe only a single peak in the 8–12GHz band. If we expect multiple frequency peaks, we have to expand the observation bandwidth. However, very high-frequency electromagnetic wave cannot penetrate ground so deep.

Then we have changed our direction. Note that, in the spatial texture case described above, we paid attention to local correlation caused by the Markovian property. In the same way, also in the frequency domain, we decided to calculate the local correlation to observe the frequency space texture in a simple manner.

Figure 5(b) illustrates our proposal, namely the frequency-domain local correlation method, to extract the frequency-domain feature. We define our new K_f as

$$\boldsymbol{K}_f = [K_f(f_1), \cdots, K_f(f_{N-1})] \tag{11}$$

$$K_f(f_n) = \frac{1}{L^2}\sum_{l_x=1}^{L}\sum_{l_y=1}^{L} z(l_x,l_y,f_n)z^*(l_x,l_y,f_{n+1}) \tag{12}$$

where $\boldsymbol{K}_f$ is the feature vector representing the correlation coefficients between the data at adjoining frequency points. This method enables us to eliminate the base frequency f_b, which means that we do not need to choose a special frequency. To extend this f_b-free advantage further, we also modify M and $K_s(i, j)$ slightly as

$$M = \frac{1}{L^2N}\sum_{l_x=1}^{L}\sum_{l_y=1}^{L}\sum_{n=1}^{N} z(l_x,l_y,f_n) \tag{13}$$

$$K_s(i,j) = \frac{1}{L^2N}\sum_{l_x=1}^{L}\sum_{l_y=1}^{L}\sum_{n=1}^{N} z(l_x,l_y,f_n)z^*(l_x+i,l_y+j,f_n) \tag{14}$$

That is, M and $\boldsymbol{K}_s$ are averaged for the all used frequency data.

The frequency-domain local correlation method is suitable for the processing in this system. Instead of the radar cross section, we use the texture of complex amplitude when we distinguish plastic landmines and other objects such as metal fragments and stones. If we can obtain a sufficiently high resolution in real-space and frequency domains, we should take into account the correlation between one pixel and another at a certain distance. However, when the system has only a low resolution, it is more effective to concentrate on the correlation between neighboring pixels, in which we can expect useful correlation information.

Additionally, in the proposed method, it is a great merit that we do not need the base frequency f_b, which was required in the conventional method. Previously we have a number of possible f_b. As presented below, it is a problem that a different f_b results in a different segmentation image. The new method is free from this problem because we have only one way to construct $\boldsymbol{K}$.

4. Experiments and results

Table 1 shows the parameters used in the following experiments. We have determined the values of $\alpha(0)$ and $\beta(0)$ empirically. We bury a mock plastic landmine under ground iteratively. We change the burial situation every time, including the ground surface and underground. The surface-roughness amplitude is about 2cm peak-to-peak. In any case, the landmine is buried at around the center of the observation area.

Figure 6(a) shows an experimental result (Result 1). The numbers show the observation frequencies. The upper blue maps show the amplitude data, while the lower color maps show the phase data. Scales of amplitude and phase are shown at the top. The position in every map corresponds to the position in real space. As mentioned above, we use these complex amplitude data obtained at the 10 frequency points.

Figure 6 (b) shows segmented images generated with the previous method. The numbers are base frequencies f_b used respectively. We can choose feature vectors $\boldsymbol{K}$ in 10 ways because there are 10 possible f_b. Each gray level indicates one of the 10 classes. We can find a segmented area at the buried plastic landmine position at f_b=8GHz and 8.8GHz. However, we cannot at other f_b.

Target (Plastic landmine)	
Size	78mm^{ϕ}, 40mm high
Burial depth	$2 \sim 3$cm
System	
Antenna height	$2 \sim 3$ cm above ground
Window size	$L = 4$
Frequency number	$N = 10$
Class number	$C = 10$
Initial learning coefficients	$\alpha(0) = 0.4$
	$\beta(0) = 0.1$
Maximum learning iteration	$TMAX = 10$

Table 1. Parameters of target and system (Nakano & Hirose, 2009).

Figure 6 (c) shows the result of segmentation by utilizing the SOM-space topology in the CSOM adaptive classification. We find that there are more classes used in the classification, i.e., 10 classes in most cases, than that in the case of the previous method. We can confirm that we can classify the landmine area appropriately at most f_b. For example, also at 8.4GHz and 9.2GHz, we are successful in the segmentation this time. These results reveal that we can improve the performance of classification by the utilization of the SOM-space topology in the CSOM.

Figure 6 (d) shows the segmentation result obtained by the frequency-domain local correlation method as well as the utilization of SOM-space topology. As mentioned before, there is only one manner to extract feature vectors $\boldsymbol{K}$ in this proposed method because we have no f_b. Here we show four result examples for various initial reference vectors in the CSOM since the result of the CSOM may depend on the initial reference-vector values. In all the cases, the landmine area is segmented correctly. We confirm a high robustness of the present method with the two proposal.

Figure 7(a) shows a measurement result (Result 2) in a different situation from that of Fig.6(a). The landmine classification seems more difficult in this case than that of Fig.6 because the calibration of direct coupling components (Masuyama et al., 2007) is somewhat sensitive to noise, occasionally resulting in insufficient compensation of antenna-selection-mode dependent amplitude.

Figure 7(b) shows the segmented images obtained with the previous method. We can classify the landmine area only when f_b=9.2GHz. We completely failed in the segmentation at other f_b. Figure 7(c) shows a result by utilizing the SOM-space topology in the CSOM. We can segment the landmine area only at 9.2GHz again.

Figure 7 (d) shows the results obtained by employing the two proposed methods. It is confirmed that we can classify the landmine area perfectly. We show four results for various initialization again. The results indicate that we can segment landmine areas stably.

In addition, we recognize that more classes are used for the classification in Fig.7(d) than in Fig.7(c) despite we use the same dynamics for the classification in the CSOM. For this reason, we can extract more characteristic feature quantities with the frequency-domain local correlation method than that with the previous one.

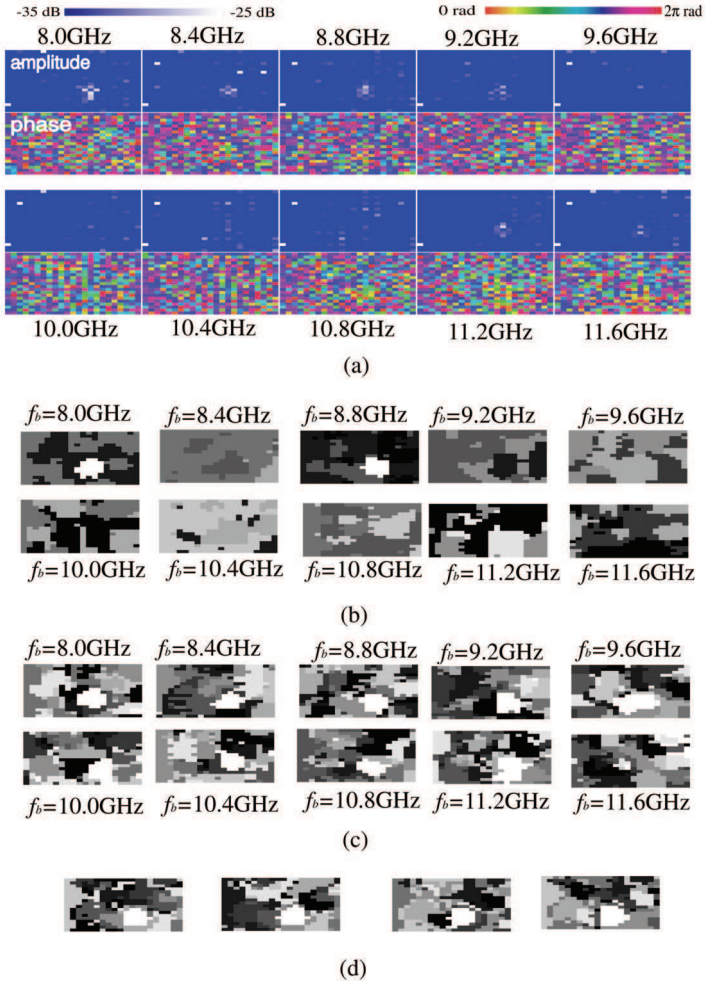

Fig. 6. Experimental results 1. (a)Amplitude and phase images at 10 frequency points, (b)classification results with the previous method. Numbers denote base frequency f_b, (c)classification results with utilization of SOM-space topology in the CSOM. Numbers denote base frequency. (d)Classification results with utilization of SOM-space topology in the CSOM and frequency-domain local correlation method. The four images show the results with various initial reference vectors in the CSOM (Nakano & Hirose, 2009).

5. Summary

In this chapter, first we explained the ground-penetrating radars (GPRs) which are studied currently as a new technology for the antipersonnel plastic landmine detection. In this field, researchers usually choose a measurement type from the pulse GPR or the stepped frequency GPR. Though both of these methods have merits and demerits, a stepped-frequency GPR has an advantage in the high ability to extract features over a pulse GPR.

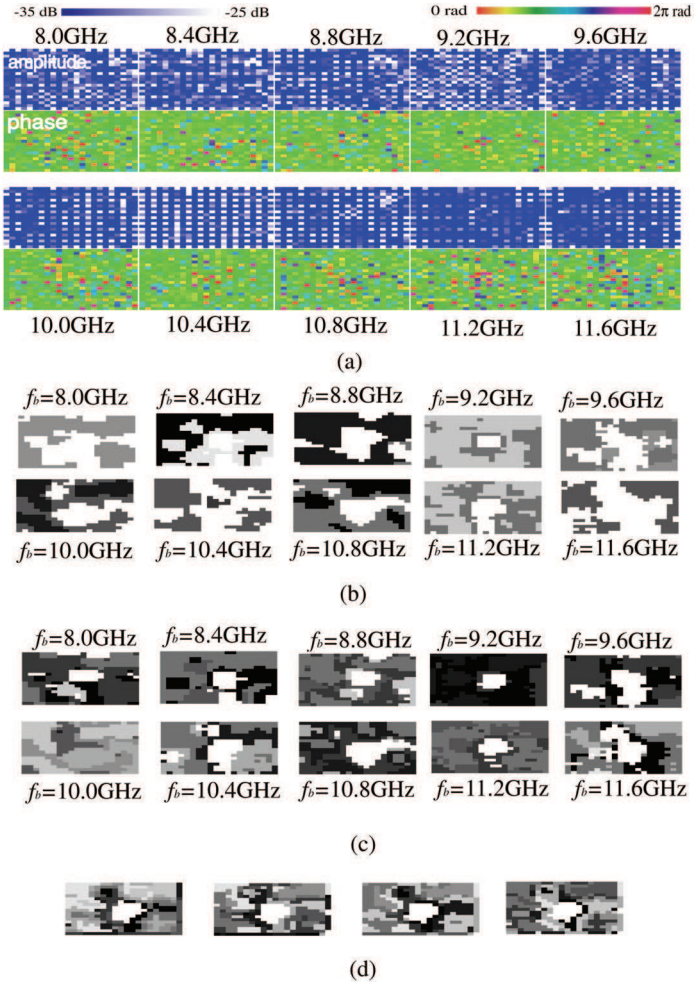

Fig. 7. Experimental results 2. (a)Amplitude and phase images at 10 frequency points, (b)classification results with the previous method. Numbers denote base frequency f_b, (c)classification results with utilization of SOM-space topology in the CSOM. Numbers denote base frequency. (d)Classification results with utilization of SOM-space topology in the CSOM and frequency-domain local correlation method. The four images show the results with various initial reference vectors in the CSOM (Nakano & Hirose, 2009).

Next, we described two techniques, which is based on the stepped-frequency GPR, to improve the performance of the GPR system to visualize plastic landmines. One is to utilize SOM-space topology in the CSOM adaptive classification to stabilize the classification process. Unlike the K-means algorithm, we can use most of the prepared classes in the learning vector quantization. The other technique is to employ local correlation as the feature vector components in the frequency domain. It extracts complex texture information better and, at the same time, eliminates the base frequency, which had to be chosen by the

user as one of the tuning parameters. Experimental results demonstrated better and stable visualization of the plastic landmine.

6. References

Bourgeois, J. M. & Smith, G. S. (1998). A complete electromagnetic simulation of the separatedaperture sensor for detecting buried land mines, *IEEE Trans. Antenna and Propagation* 46(10): 1419–1426.

Hara, T. & Hirose, A. (2004). Plastic mine detecting radar system using complex-valued selforganizing map that deals with multiple-frequency interferometric images, *Neural Networks* 17(8-9): 1201–1210.

Hara, T. & Hirose, A. (2005). Adaptive plastic-landmine visualizing radar system: effects of aperture synthesis and feature-vector dimension reduction, *IEICE Transactions on Electronics* E88-C(12): 2282–2288.

Hirose, A. (ed.) (2003). *Complex-Valued Neural Networks: Theories and Applications*, World Scientific Publishing Co. Pte. Ltd.

Hirose, A. (ed.) (2006). *Complex-Valued Neural Network*, Heidelberg: Springer-Verlag.

Hirose, A., Toh Jiayun, A. & Hara, T. (2005). Plastic landmine identification by multistage association, *IEICE Tech. Rep.* (NC2004-156).

Kobayashi, T., Feng, X.&Sato, M. (2004). Agpr for landmine detection using an array antenna, *International Symposium on Antennas and Propagation (ISAP) Sendai*.

Masuyama, S. & Hirose, A. (2007). Walled LTSA array for rapid, high spatial resolution, and phase sensitive imaging to visualize plastic landmines, *IEEE Transactions on Geoscience and Remote Sensing* 45(8): 2536–2543.

Masuyama, S., Yasuda, K. & Hirose, A. (2007). Removal of direct coupling in a walled-LTSA array for visualizing plastic landmines, *International Symposium on Antennas and Propagation (ISAP) 2007 Niigata*, pp. 1238–1241.

Montoya, T. P. & Smith, G. S. (1999). Land mine detection using a ground-penetrating radar based on resistively loaded vee dipoles, *IEEE Trans. Antenna and Propagation* 47(12): 1795–1806.

Moriyama, T., Nakamura, M., Yamaguchi, Y. & Yamada, H. (1997). Radar polarimetry applied to the classification of target buried in the underground,*Wideband Interferometric Sensing and Imaging Polarimetry*, Vol. 3210 of *Proc. of SPIE*, pp. 182–189.

Nakano, Y. & Hirose, A. (2009). Improvement of plastic landmine visualization performance by use of ring-csom and frequency-domain local correlation, *IEICE Transactions on Electronics* E92-C(1): 102–108.

Peters Jr., L. & Daniels, J. J. (1994). Ground penetrationg radar as a surface environmental sensing tool, *Proceedings of the IEEE*, Vol. 82,No.12, pp. 1802–1822.

Sato, M. (2005). Dual sensor alis evaluation test in afghanistan, *IEEE Geoscience and Remote Sensing Society Newsletter* pp. 22–24.

Sato, M., Hamada, Y., Feng, X., Kong, F.-N., Zeng, Z. & Fang, G. (2004). GPR using an array antenna for landmine detection, *Near Subsurface Geophysics* 2: 7–13.

Sato, M., Takahashi, K., Feng, X. & Kobayashi, T. (2006). Stepped-frequency handheld demining dual sensor alis, *Proceeding of 11th International Conference on Ground Penetrating Radar*, p. UXO.10.

Sato, M. & Takeshita, M. (2000). Estimation of subsurface fracture roughness by polarimetric borehole radar, *IEICE Trans. Electron.* E83-C(12): 1881–1888.

Shrestha, S. M., Arai, I. & Tomizawa, Y. (2004). Landmine detection using impulse ground penetrating radar, *Internationall Symposium on Antennas and Propagation (ISAP) Sendai*.

Radar Technology

Edited by Guy Kouemou

ISBN 978-953-307-029-2
Hard cover, 410 pages
Publisher InTech
Published online 01, January, 2010
Published in print edition January, 2010

In this book “Radar Technology”, the chapters are divided into four main topic areas: Topic area 1: “Radar Systems” consists of chapters which treat whole radar systems, environment and target functional chain. Topic area 2: “Radar Applications” shows various applications of radar systems, including meteorological radars, ground penetrating radars and glaciology. Topic area 3: “Radar Functional Chain and Signal Processing” describes several aspects of the radar signal processing. From parameter extraction, target detection over tracking and classification technologies. Topic area 4: “Radar Subsystems and Components” consists of design technology of radar subsystem components like antenna design or waveform design.

InTech Europe
University Campus STeP Ri
Slavka Krautzeka 83/A
51000 Rijeka, Croatia
Phone: +385 (51) 770 447
Fax: +385 (51) 686 166
www.intechopen.com

InTech China
Unit 405, Office Block, Hotel Equatorial Shanghai
No.65, Yan An Road (West), Shanghai, 200040, China
中国上海市延安西路65号上海国际贵都大饭店办公楼405单元
Phone: +86-21-62489820
Fax: +86-21-62489821